Electronic Supplementary Material (ESI) for Nanoscale.

Supplementary Information

Carrier scattering in quasi-free standing graphene on hexagonal boron nitride

Sun Jun Kim§, Byeongho Park§, Seung Hyo Noh, Hyong Seo Yoon, Juyeong Oh, SangHyuk Yoo, Keonwook Kang, Byungchan Han and Seong Chan Jun*,

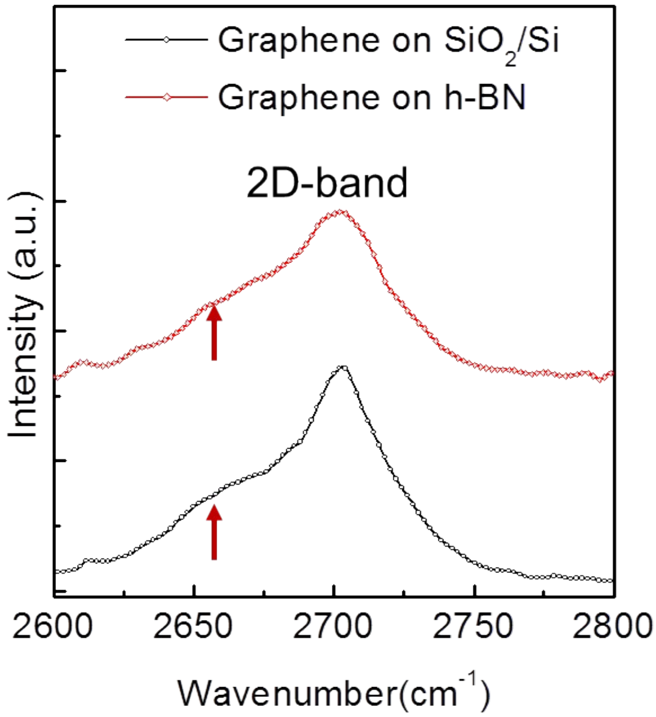

Fig. S1 Raman shift of graphene on SiO_2/Si and h-BN in our devices.

The number of Graphene layers was analyzed by Raman spectroscopy. In our devices, graphene on SiO_2/Si and h-BN exhibited considerably similar feature from 2600 to 2800 cm^{-1}. In 2D-band, the main peak at 2700 cm^{-1} and shoulder peak at 2660 cm^{-1} were observed, which indicate we used 2-4 layers of graphene with AFM images in Fig. 1. [1]

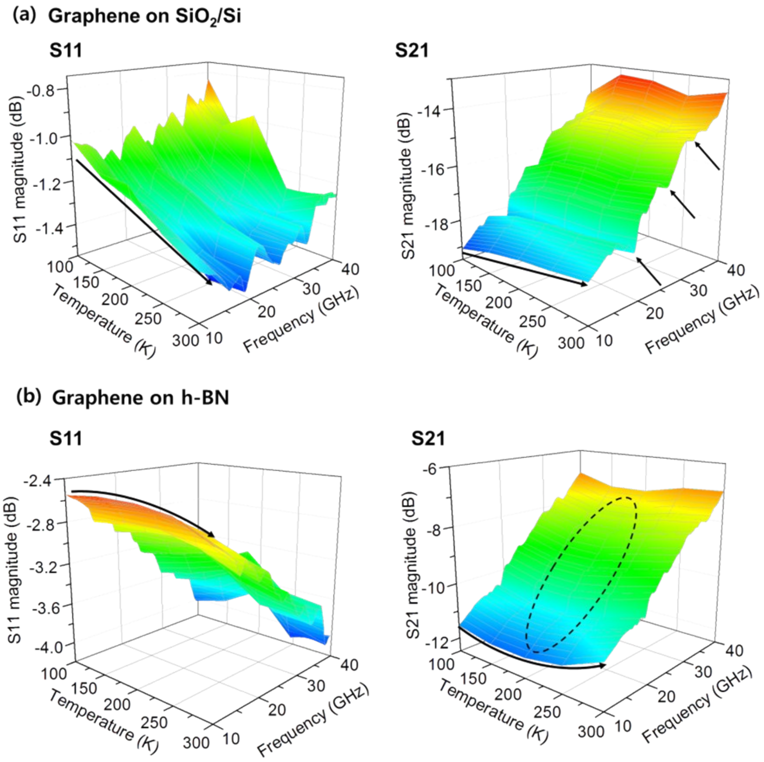

Fig. S2 Variation of S-parameters, S11 (reflection), and S21 (transmission) with experimental temperature and frequency; graphene on (a) SiO_2/Si and (b) h-BN

The S11 magnitude of graphene on SiO_2/Si linearly decreased with increasing temperature. On the other hand, S21 magnitude showed with the complete opposite to the S11 result. Disorder of the graphene induced by SiO_2 substrate resulted in trapped charges in its surface, which provided the depressions at 20 GHz, 30 GHz, and 35 GHz in S21 magnitude. In the S-parameters of graphene on h-BN, the magnitude reversed at a characteristic temperature near 180 K; S11 magnitude increased up to 180 K and then decreased, but the S21 magnitude behaved in an opposite manner to the S11 magnitude.

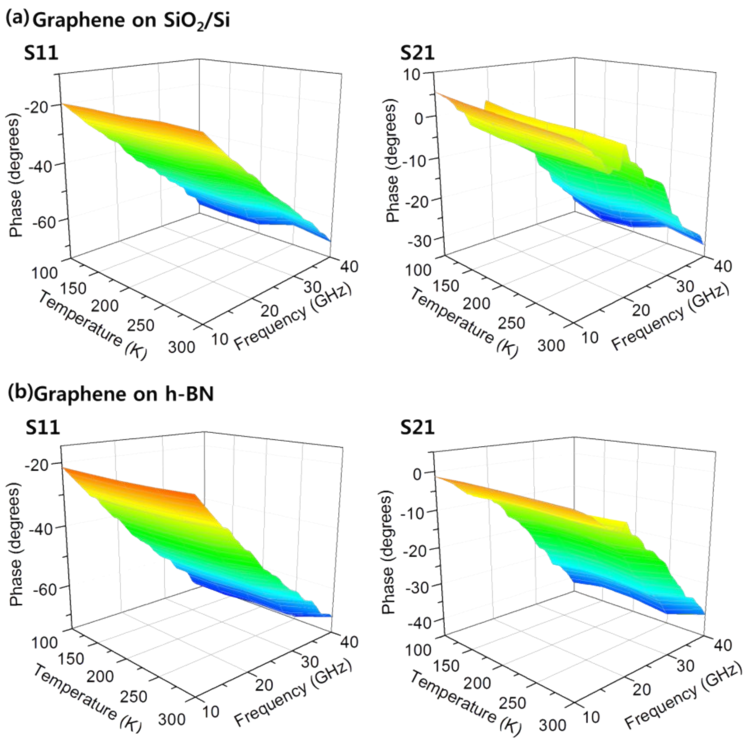

Fig. S3 Phases of devices, graphene on (a) SiO_2/Si and (b) h-BN, with experimental temperatures and frequency.

The S-parameters and phases (Fig. S3) of RF can be converted to the following matrix equations,

$$S_{ij} = S_{Magnitude,ij} e^{i\theta_{Phase,ij}} (i, j = 1, 2) \quad \text{and} \tag{1}$$

$$\begin{bmatrix} A & B \\ C & D \end{bmatrix} = \frac{1}{2S_{21}} \begin{bmatrix} (1 - S_{11}^2 + S_{21}^2) & Z_0((1 + S_{11}^2)^2 - S_{21}^2 \\ \frac{1}{Z_0}((1 - S_{11})^2 - S_{21}^2) & (1 - S_{11}^2 + S_{21}^2) \end{bmatrix} \quad , \tag{2}$$

where Z_0 (50 Ω) denotes the initial load for GSG probing.[2-4] Then the RF propagation constant γ and impedance Z are extracted from the following relationship for RF transmission,

$$\gamma = \cos^{-1} A , \qquad Z = \sqrt{\frac{B}{C}} \ . \tag{3}$$

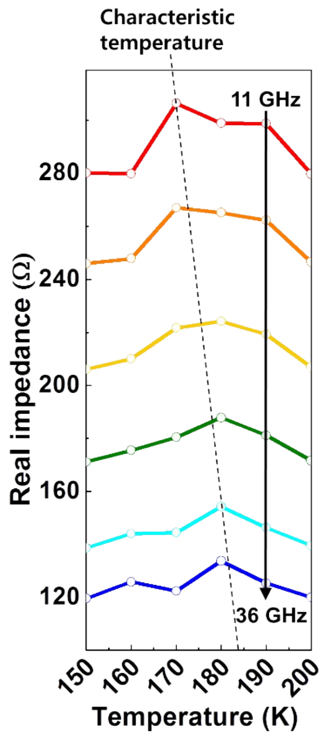

Fig. S4 Real impedance of graphene on h-BN from 150 to 200 K

The real impedance of graphene on h-BN from 150 to 200 K represented in Fig. S4 in order to investigate the highest impedance, which moved from 170 to 180 K as the frequency increased from 11 to 36 GHz. The impedance peak was shifted because Dirac fermion electrical transport mainly contributed to the free carrier response at low frequency range, the impedance peak was shifted. [5] So, thermally generated carriers (free carrier response) were more dominant than scattering effect at a low frequency, and thus the impedance peak shifted to lower temperature with decreasing frequency.

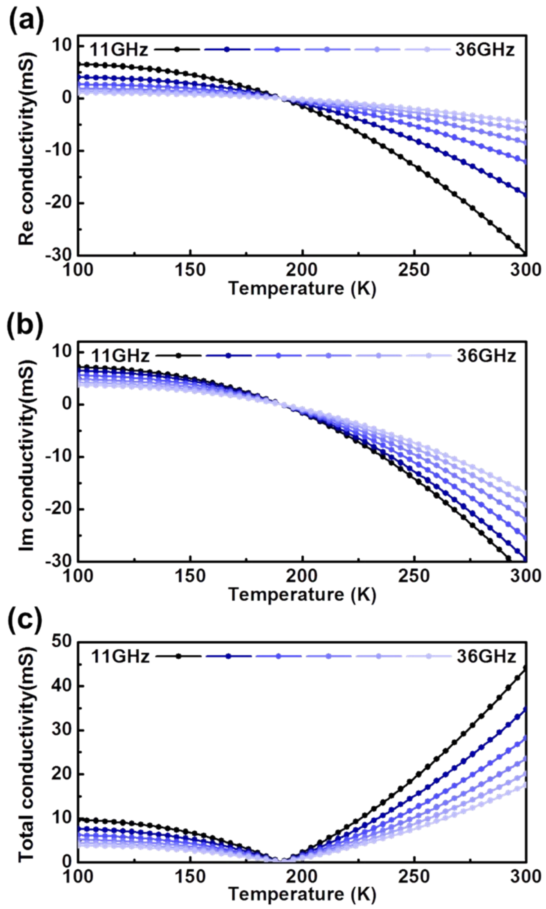

Fig. S5 The Kubo formalism result of intrinsic graphene. Calculated (a) Real, (b) imaginary and (c) total conductivity of graphene.

The real (Fig. S5(a)) and imaginary (Fig. S5(b)) part of conductivity are rapidly decreased, and total conductivity (Fig. S5(c)) is conversed from negative to positive gradient after 180K. These results are calculated by Kubo formalism with equation 3 of manuscript in order to comparing impedance result (Fig. 5)

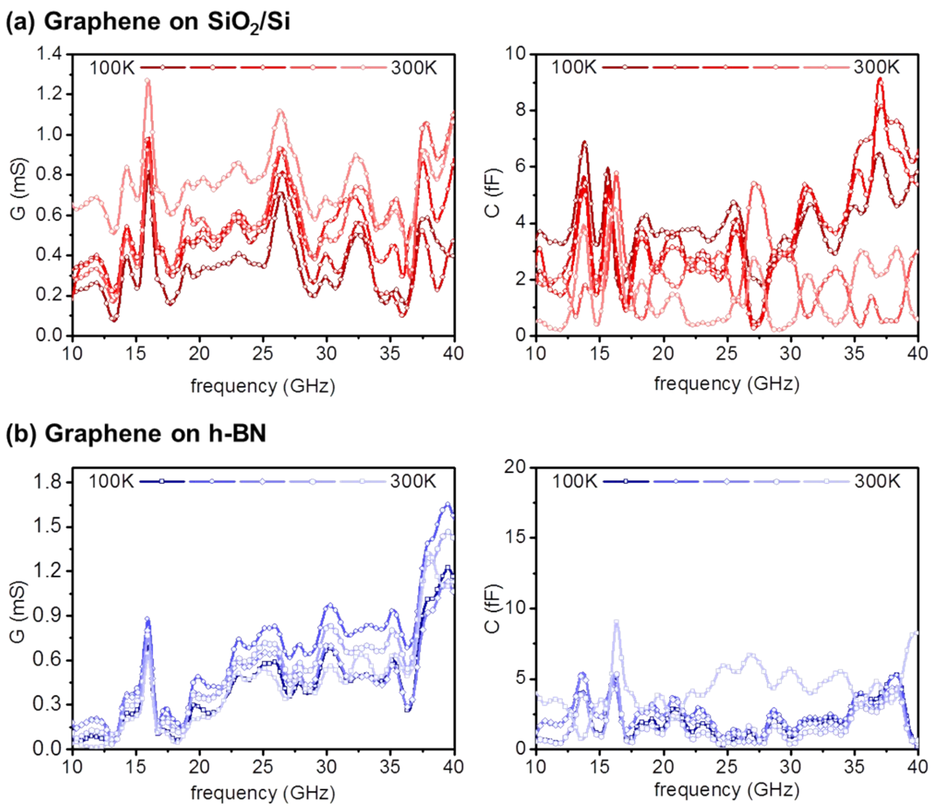

Fig. S6 Extracted shunt conductance and shunt capacitance of graphene on (a) SiO_2/Si and (b) h-BN from 100 K to 300 K

The shunt conductance (G) and shunt capacitance (C) from 100 K to 300 K are shown in Fig. S6. While the resistance (R) and inductance (L) have linear characteristics with temperature as in Fig. 6, the G and C show nonlinear characteristics. The temperature dependence of G and C is relatively small, which demonstrates that the electrical effects of the SiO_2/Si and h-BN on graphene as a substrate are quite similar.

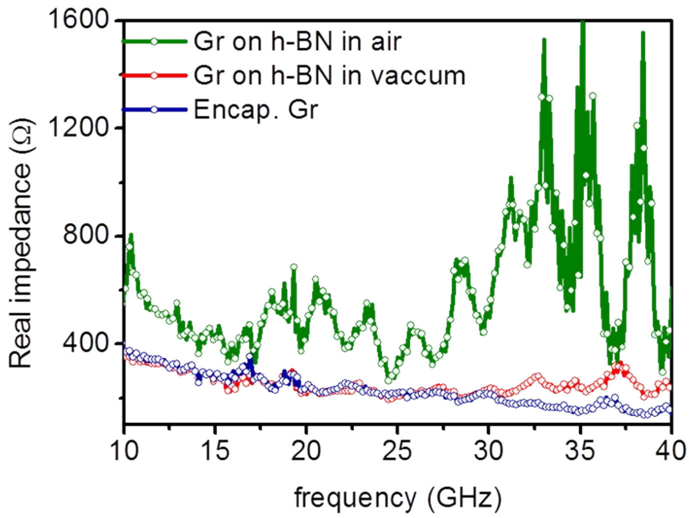

Fig. S7 The real impedance of graphene on h-BN in air, graphene on h-BN in vacuum, and encapsulated graphene.

The real impedance of graphene on h-BN in air, vacuum, and encapsulated represented in Fig. S7. The real impedance of graphene on h-BN in air is higher than the other samples, which is caused by interaction between the graphene surface and air. The scattering effect in air cause large fluctuations from 30 to 40 GHz. The graphene on h-BN in vacuum and encapsulated graphene show very similar low real impedance magnitude values, because both of samples do not interact with the graphene surface and air.

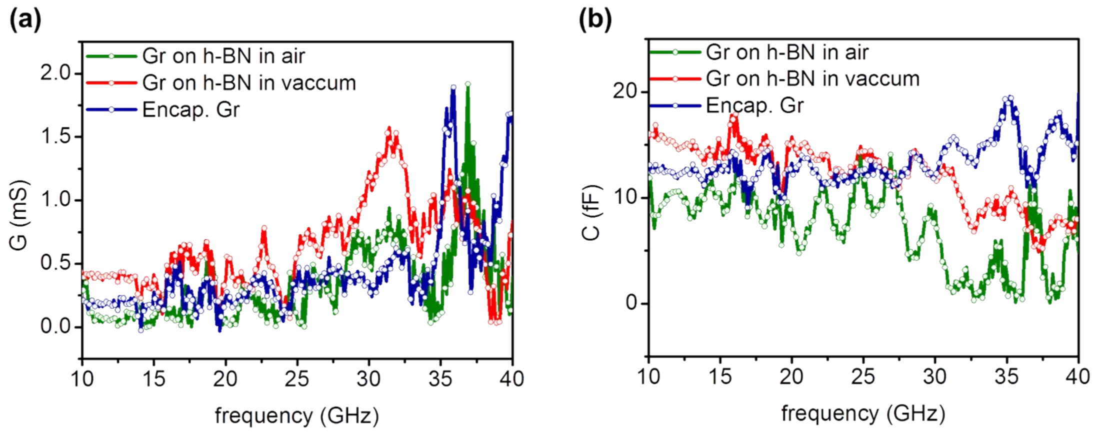

Fig. S8 The (a) shunt conductance and (b) shunt capacitance of graphene on h-BN in air, graphene on h-BN in vacuum, and encapsulated.

The shunt conductance (G) and shunt capacitance (C) of graphene on h-BN in air, vacuum, and encapsulated are exhibited in Fig. S8. While the resistance (R) and inductance (L) have distinct characteristics between samples in Fig. 7(f) and (g) of manuscript, the G and C show confused characteristics. The difference of G and C between the different sample types is considerably smaller than the difference for R and L, demonstrating the insignificant effect of air on these electrical characteristics.

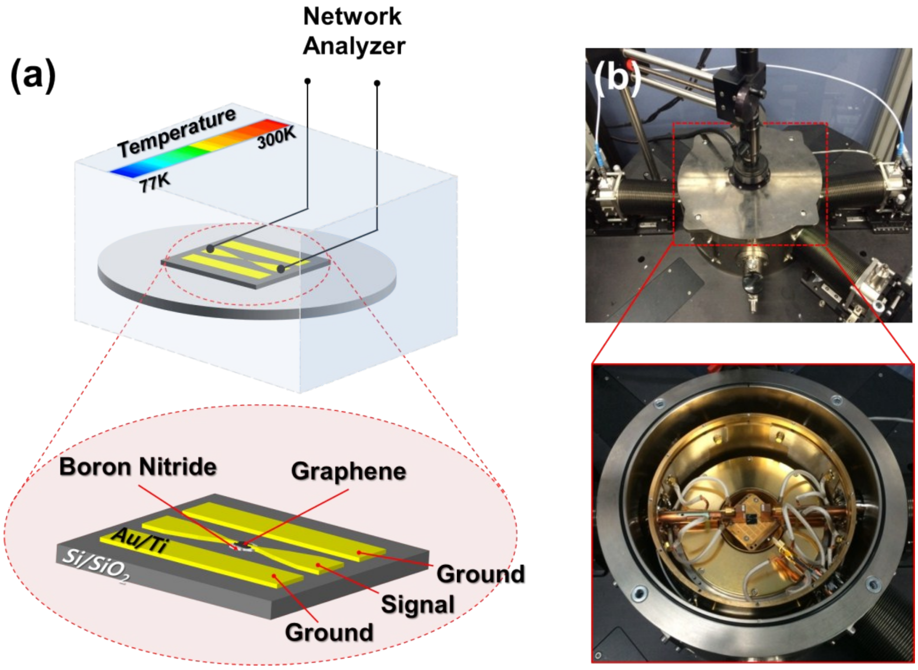

Fig. S9 GSG pattern and radio frequency measurements. (a) The schematic of radio frequency measurement system with different temperature and structure for GSG pattern. (b) Image of experiment setting in vacuum chamber

RF signals of devices were measured under vacuum conditions in order to prevent water vapor and impurities in the air condensing. The liquid nitrogen flowed around the vacuum chamber, which gradually lowered the temperature on the supporting stage of the measurement system. Then, current was applied slowly to thermal lines and the specific temperature in the chamber controlled using a proportional integral derivative controller (PID control).

Supplementary reference

1. Y. Wang, Z. hua Ni, T. Yu, Z. Xiang Shen, H. min Wang, Y. hong Wu, W. Chen and A. Wee, Raman Studies of Monolayer Graphene: The Substrate Effect, 2008.

2. L. N. Dworsky, Modern transmission line theory and applications, RE Krieger Pub. Co.1979.

3. W. R. Eisenstadt and Y. Eo, Components, Hybrids, and Manufacturing Technology, IEEE Transactions on, 1992, 15, 483-490.

4. S. C. Jun, J. Choi, S. Cha, C. Baik, S. Lee, H. J. Kim, J. Hone and J. Kim, Nanotechnology, 2007, 18, 255701.

5. J. Horng, C.-F. Chen, B. Geng, C. Girit, Y. Zhang, Z. Hao, H. A. Bechtel, M. Martin, A. Zettl and M. F. Crommie, Physical Review B, 2011, 83, 165113.